Journal of Materials Chemistry C

ROYAL SOCIETY OF CHEMISTRY

PAPER

View Article Online
View Journal | View Issue

Cite this: J. Mater. Chem. C, 2023, 11, 11213

Antiferromagnetic ordering and signatures of enhanced spin-frustration in honeycomb-layered tellurates with Ag bilayers†

Sachio Komori, *[a] Kohei Tada, *[b] Noboru Taguchi, [b] Tomoyasu Taniyama [a] and Titus Masese *[b]

A low-dimensional magnetic system promotes strong interactions between quantum spins and leads to fascinating quantum phenomena. To realize quantum devices based on the spin-liquid ground state, a two-dimensional magnetic system with strong spin-frustration is highly desired. A honeycomb-layered tellurate with a 3d transition metal within its slabs is a potential system that can host Kitaev quantum spin-liquid although conclusive evidence for the spin-liquid phase has not been reported to date. This might be partially due to the presence of an interslab exchange coupling between magnetic honeycomb slabs which stabilizes antiferromagnetic ordering and potentially suppresses Kitaev interactions. Here, we report the magnetic and spin frustration properties of Ag-based honeycomb layered tellurates with magnetic honeycomb slabs separated by Ag bilayers which are expected to screen the interslab exchange coupling. From magnetization measurements, we observe antiferromagnetic ordering and signatures of enhanced spin-frustration for the tellurates containing Ag-bilayers relative to other honeycomb layered tellurates without bilayers. The results might be promising for the realization of the Kitaev quantum spin liquid.

Received 2nd June 2023,
Accepted 25th July 2023

DOI: 10.1039/d3tc01915b

rsc.li/materials-c

Introduction

Spin-frustration in a magnetic material enables quantum spins to have a liquid-type of ground state instead of a solid-type.[1,2] In a Kitaev spin model,[3–5] bond-dependent Ising interaction of spins in a two-dimensional (2D) honeycomb lattice leads to spin-frustration and a quantum entangled spin-liquid ground state with a number of spin configurations of the order of Avogadro's number. In such a system, the spin Hamiltonian is fractionalized into the hopping Hamiltonian of Majorana fermions and therefore, fluctuating spins can be described by a propagation of Majorana fermions.[6,7]

To realize the bond-dependent anisotropic Ising interaction, spins need to be coupled with spatially anisotropic orbitals *via* strong spin–orbit coupling.[8] Based on the concept, a lot of research has been undertaken to realize a Kitaev spin-liquid in a honeycomb-structured material with 4d and 5d heavy metals with strong spin–orbit coupling. To date, iridates[9] and α-$RuCl_3$[10] are strong candidates of a Kitaev material although a spin-liquid ground state at sufficiently low temperatures has not been identified in these systems. This is attributed to long-range magnetic order such as Heisenberg interactions that perturb Kitaev interactions. Hence, a magnetic honeycomb lattice with localized (short-range) 3d-orbitals,[11] albeit relatively weak spin–orbit coupling, is attracting attention as a possible Kitaev system especially after $Na_3Co_2SbO_6$ was reported to potentially host a Kitaev spin-liquid state.[12] Recently, the presence of strong spin-frustration has been reported in $Na_3Co_2SbO_6$ and $Na_2Co_2TeO_6$[13,14] and a detailed comparison with other 3d honeycomb layered oxides having different crystal structures has been a subject of increasing interest.

A honeycomb layered tellurate $A_2M_2TeO_6$, where A is typically an alkali metal (*e.g.*, A = Li, Na, K) and M is typically a 3d transition metal (*e.g.*, M = Ni, Co), has a 2D honeycomb lattice that can potentially host the Kitaev spin liquid state. So far, antiferromagnetic (AFM) transition with the Néel temperature (T_N) below 35 K has been reported for $Na_2Co_2TeO_6$,[15–20] $Na_2Ni_2TeO_6$,[15,19–24] $K_2Ni_2TeO_6$,[25,26] and $Li_2Ni_2TeO_6$,[26] in which (Te, Co)–O and (Te, Ni)–O honeycomb layers are responsible for the AFM ordering. However, there have been limited reports on spin-frustration in the 2D magnetic honeycomb layers.[13,14] This would be partially due to an interslab exchange coupling in honeycomb layered tellurates that stabilizes AFM ordering. In addition, degradation of

[a] Department of Physics, Nagoya University, Furo-cho, Chikusa-ku, Nagoya 464-8602, Japan. E-mail: komori.sachio.h0@f.mail.nagoya-u.ac.jp
[b] Research Institute of Electrochemical Energy, National Institute of Advanced Industrial Science and Technology, 1-8-31 Midorigaoka, Ikeda, Osaka 563-8577, Japan. E-mail: k-tada@aist.go.jp, titus.masese@aist.go.jp

† Electronic supplementary information (ESI) available. See DOI: https://doi.org/10.1039/d3tc01915b

magnetic properties due to moisture absorption can suppress spin-frustration.

Here, we report magnetic properties of Ag-based honeycomb-layered tellurates: global composition $Ag_2M_2TeO_6$ (M = Co, $Co_{0.5}Ni_{0.5}$, and Ni) consisting of Ag-rich $Ag_6M_2TeO_6$ with a Ag-bilayer and Ag-deficient $Ag_{2-x}M_2TeO_6$ ($0 < x \leq 2$) with a Ag-monolayer, which are robust against degradation of magnetic properties due to the absence of hygroscopicity. To date, there has been no report on magnetic properties of Ag-based honeycomb layered tellurates, especially honeycomb layered tellurates containing Ag bilayers. From temperature and field dependent magnetization measurements, we observe antiferromagnetic ordering and signatures of spin-frustration in the vicinity of the antiferromagnetic phase transition which might result from enhanced 2D magnetic ordering due to the screening of the interslab exchange coupling by the Ag bilayers.

Results and discussion

Fig. 1(a)–(d) show typical high-angle annular dark-field scanning transmission electron microscopy (HAADF-STEM) images of $Ag_2Ni_2TeO_6$, which confirm the coexistence of dominant $Ag_6Ni_2TeO_6$ phase with a Ag-bilayer and partial $Ag_{2-x}Ni_2TeO_6$ ($0 < x \leq 2$) phase with a Ag-monolayer. Unlike other tellurates, in $Ag_{2-x}M_2TeO_6$ ($0 < x \leq 2$) (M = Co, $Co_{0.5}Ni_{0.5}$, and Ni), a straight dumbbell-like coordination between the d-orbitals of Ag^+ and the 2p-orbitals of O^{2-} along the interslabs enhances the interslab distance between the (Te, M)–O layers.[27] In addition, the formation of Ag-bilayers recently discovered[28] further extends the interslab distance relative to its monolayered counterpart. It has been recently theorized that a weak attractive interaction between Ag atoms constituting argentophilicity resulting from pseudo-spin symmetry is responsible for the unconventional formation and stability of the Ag bilayers.[27,28]

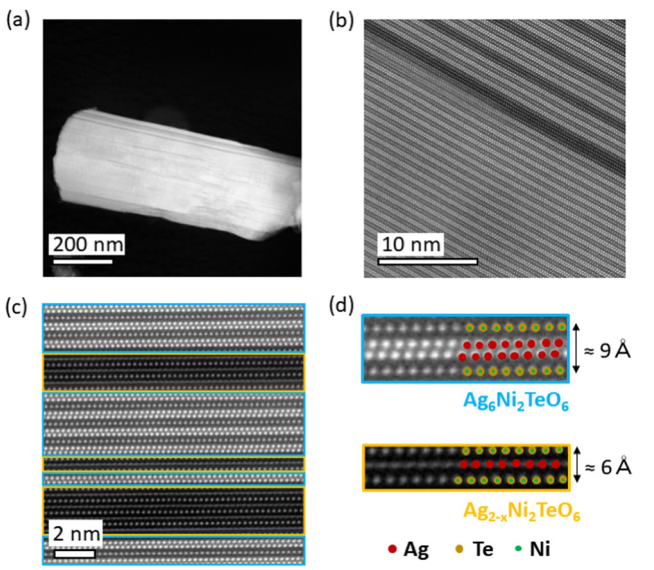

Fig. 1 (a)–(c) HAADF-STEM images of $Ag_2Ni_2TeO_6$ with various magnifications. Blue and yellow squares in (c) indicate the areas of $Ag_6Ni_2TeO_6$ and $Ag_{2-x}M_2TeO_6$ ($0 < x \leq 2$), respectively, which are magnified in (d).

In Fig. 2(a)–(c), we plot the magnetic susceptibility (χ) *versus* temperature (T) curves at the magnetic field (H) of 100 Oe for polycrystalline powders of global composition $Ag_2M_2TeO_6$ with M = Co, $Co_{0.5}Ni_{0.5}$, and Ni, respectively. An AFM transition is observed for all the samples. T_N (defined as T at which $d\chi/dT$ becomes maximum) increases with the Ni concentration and becomes highest for M = Ni (see Table 1 for the summary of the magnetic properties). The discrepancy between the zero-field-cooling (ZFC) and the field-cooling (FC) curves below T_N and the rise of χ at $T \approx 0$ for M = Co imply the presence of a small fraction of ferromagnetic (non-AFM) phase. The behaviors are less pronounced for M = $Co_{0.5}Ni_{0.5}$ and Ni, suggesting less amount of the non-AFM phase for higher Ni concentration, which might be related to higher T_N. However, the possible presence of spin-glass state originating from spin-frustration could also lead to the discrepancy and the rise of χ at $T \approx 0$ and further investigation is necessary to clarify the origin.

By fitting ZFC curves of $\chi^{-1}(T)$ [see Fig. 2(d)] above $T = 60$ K to the Curie–Weiss law [see the dashed curves in Fig. 2(d)], we estimate the Curie–Weiss temperatures (T_{CW}) of (-26.4 ± 0.7) K, (-40.8 ± 0.6) K, and (-84.3 ± 0.9) K and the effective paramagnetic moments (μ_{eff}) of $7.58\mu_B$, $6.62\mu_B$, and $5.78\mu_B$ for M = Co, $Co_{0.5}Ni_{0.5}$, and Ni, respectively. The experimentally obtained μ_{eff} values are close to the theoretical values of $7.74\mu_B$ (M = Co), $6.70\mu_B$ (M = $Co_{0.5}Ni_{0.5}$), and $5.66\mu_B$ (M = Ni) calculated from the moment of Co^{2+} ($3.87\mu_B$) and Ni^{2+} ($2.83\mu_B$) free ions, suggesting that the magnetic moment of the samples is predominated by unpaired spins of Co^{2+} and Ni^{2+} ions, whilst the magnetic moment of pseudo-spins of the Ag-bilayers is rather small (see supplementary materials for a control measurement on the global composition $Ag_2Mg_2TeO_6$ with dominant domains of the bilayered $Ag_6Mg_2TeO_6$), suggesting that the pseudo-spin magnetic moment (if present) may be of a different character (such as in graphene[29]) from conventional magnetic moments measured in our experiment. The upward deviation of $\chi^{-1}(T)$ curves from the Curie–Weiss law below $T = 60$ K [see inset in Fig. 2(d)] suggests the presence of the ferromagnetic exchange interaction that might be a signature of quantum spin liquid, which we will discuss later.

In Fig. 2(e), we plot $d\chi/dT$ *versus* T for M = Co, $Co_{0.5}Ni_{0.5}$, and Ni. The width of the AFM transition (ΔT_N) estimated from the temperatures giving the maximum and zero values of $d\chi/dT$ is (4.0 ± 1.0) K, (4.0 ± 1.0) K, and (10.5 ± 1.0) K for M = Co, $Co_{0.5}Ni_{0.5}$, and Ni, respectively. A broad AFM transition with large ΔT_N is observed for all the samples, which is indicative of strong 2D magnetic ordering.[22,30] Recent neutron scattering and specific heat measurements on $Na_2Co_2TeO_6$ and $Na_2Ni_2TeO_6$ have demonstrated that the broad peak of a $\chi(T)$ curve corresponds to the 2D magnetic ordering temperature within a slab.[22,31,32] The largest ΔT_N value for our M = Ni suggests an enhanced two-dimensional magnetic ordering due to a strong in-plane exchange interaction manifesting as large T_{CW}. Although the interslab exchange coupling is not negligible for tellurates with a cationic monolayer,[19,21,26] it can be strongly suppressed for

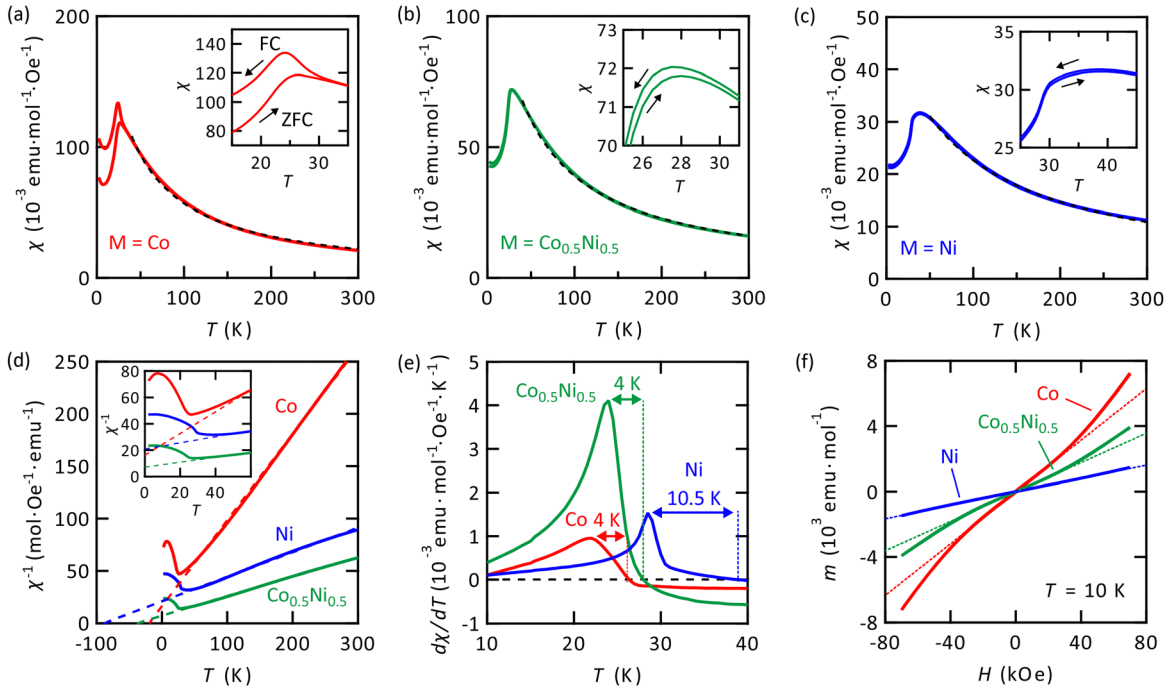

Fig. 2 Magnetic susceptibility (χ) *versus* temperature (T) of $Ag_2M_2TeO_6$ polycrystalline powders with (a) M = Co, (b) M = $Co_{0.5}Ni_{0.5}$, and (c) M = Ni at H = 100 Oe. (d) Inverse susceptibility (χ^{-1}) *versus* T for M = Co, $Co_{0.5}Ni_{0.5}$, and Ni at H = 100 Oe. The dashed curves in (a)–(d) represent a least squares regression line fit to the Curie–Weiss law, giving Curie–Weiss temperatures of −26.4 K, −40.8 K, and −84.3 K and the effective paramagnetic moments of 7.58μ_B, 6.62μ_B, and 5.78μ_B for M = Co, $Co_{0.5}Ni_{0.5}$, and Ni, respectively. The insets in (a)–(d) show the magnified curves near the AFM transition. (e) dχ/dT *versus* T and (f) magnetic moment (m) *versus* H for M = Co, $Co_{0.5}Ni_{0.5}$, and Ni. The arrows in (e) represent the width of the AFM transition, defined from the temperatures giving the maximum and zero-value of dχ/dT. The data in (d) and (e) are obtained during warming at H = 100 Oe after zero-field-cooling. The dashed lines in (f) are the guide to the eye.

Table 1 Magnetic properties of $Ag_2M_2TeO_6$ (M = Co, $Co_{0.5}Ni_{0.5}$, Ni)

	M = Co	M = $Co_{0.5}Ni_{0.5}$	M = Ni
T_N (K)	22.0 ± 0.5	24.0 ± 0.5	28.5 ± 0.5
T_{CW} (K)	−26.4 ± 0.7	−40.8 ± 0.6	−84.3 ± 0.9
C_{mol} (emu K mol^{-1})	7.19 ± 0.06	5.48 ± 0.03	4.18 ± 0.02
μ_{eff} (μ_B)	7.58 ± 0.03	6.62 ± 0.02	5.78 ± 0.02
$f = \lvert T_{CW}\rvert/T_N$	1.20 ± 0.06	1.70 ± 0.06	2.96 ± 0.08
ΔT_N (K)	4.0 ± 1.0	4.0 ± 1.0	10.5 ± 1.0

$Ag_6M_2TeO_6$ with long interslab distance mediated by Ag-bilayers (see ESI,† Fig. S1). Hence, the coexistence of the broad (2D-like) and sharp (3D-like) transitions for all the samples may be due to the coexistence of the $Ag_6M_2TeO_6$ and $Ag_{2-x}M_2TeO_6$ ($0 < x \leq 2$) phases with different interslab distance.

Fig. 2(f) shows the magnetic moment *versus* field [$m(H)$] curves at 10 K. The non-linear $m(H)$ curves for M = Co and $Co_{0.5}Ni_{0.5}$ indicate a broad spin-flop transition which can occur in AFM materials and has also been reported for other tellurates.[16,18,23] From the numerical derivative of the $\chi(H)$ curves, we find that the spin-flop transition occurs broadly around $H_{sf} \approx 6 \times 10^5$ Oe (see ESI,† for details). The absence of a spin-flop transition for M = Ni suggests that the transition field H_{sf} is higher than 70 kOe. Since H_{sf} is given as $H_{sf} = (2H_{ex}H_A)^{0.5}$ where H_{ex} is the exchange field and H_A is the anisotropy field, the large H_{sf} for M = Ni indicates the large H_{ex} and hence the stronger AFM ordering, consistent with the largest T_N for M = Ni.

We now discuss the potential existence of quantum spin-liquid originating from a 2D spin-frustrated state. Quantum criticality in a spin liquid state can be observed at the temperature range where the classical ground state is suppressed by the thermal fluctuations and gives the power law: $\chi(T) \sim T^{-\alpha}$ (α: constant) [and therefore $\log(H^{\alpha}\chi) \approx -\alpha \log(T/H)$] at temperatures slightly above T_N where the long-range Heisenberg interaction is suppressed.[7,33–37] The (H, T)-dependent χ at $T_N < T < 60$ K follows a single line with the slope of $-\alpha$ where α = 0.41, 0.34, and 0.28 for M = Co, $Co_{0.5}Ni_{0.5}$, and Ni, respectively [see Fig. 3(a)]. The variation of the critical exponent α among the three samples with different compositions might be due to different strength of quantum fluctuations. The remarkable deviation from the Curie–Weiss law (α = 1) and the scaling with the same exponent α over 3 orders of magnitude in T/H are the signatures of a spin-liquid state[36,37] in our samples. In addition, all the samples show $|T_{CW}| > T_N$, implying a suppression of T_N due to a factor that can be related to spin-frustration. The spin-frustration index $f = |T_{CW}|/T_N$ for the global composition $Ag_2M_2TeO_6$ obtained from this work (f = 1.2–3.0) is larger than that reported for $Na_2M_2TeO_6$ (f = 0.5–1.2),[15–24] $K_2M_2TeO_6$ (f = 0.6–1.1),[25,26] and $Li_2M_2TeO_6$[26] (f = 0.8) [see Fig. 3(b)]. We note that in a Kitaev system, a suppression of T_N can result from a competition between the AFM interaction and the Ising interaction within a 2D honeycomb lattice. Therefore, unlike a geometrically frustrated system the relation between

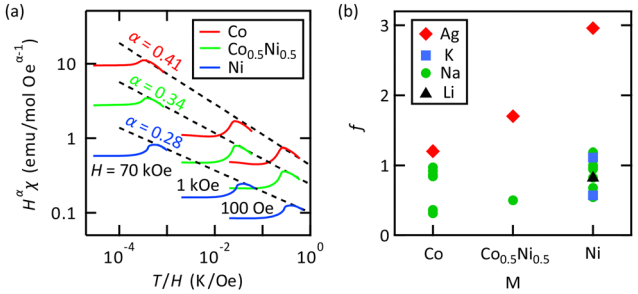

Fig. 3 (a) Scaling plot of $H^{\alpha}\chi$ *versus* T/H at various H where α = 0.41, 0.34, and 0.28 for M = Co (red curves), $Co_{0.5}Ni_{0.5}$ (green curves), and Ni (blue curves), respectively. The dashed lines show fit to the curves over the range of $T_N < T < 60$ K, giving the scaling with the same exponent α over 3 orders of magnitude in T/H. (b) The spin-frustration index f for $Ag_2M_2TeO_6$ (diamonds) from this work, $K_2M_2TeO_6$ (squares),[25,26] $Na_2M_2TeO_6$ (circles),[15–24] and $Li_2M_2TeO_6$ (triangle)[26] with M = Co, $Co_{0.5}Ni_{0.5}$, and Ni.

spin-frustration and the T_N suppression (the f value) can be complicated.

Since the interslab distance of Ag-deficient $Ag_{2-x}M_2TeO_6$ (6 Å[28]) is either comparable to or shorter than that of Na, K, and Li-based tellurates [see ESI,† Fig. S1(a)], the signatures of the enhanced 2D spin-frustration in our Ag-based tellurate can be attributed to the Ag-rich $Ag_6M_2TeO_6$ phase with remarkably long interslab distance of 9 Å,[28] which is expected to screen the interslab magnetic exchange coupling. From density functional theory (DFT) simulations of the total energy difference between layered-antiferromagnetic and ferromagnetic ordering, we find that the interslab magnetic exchange coupling of honeycomb layered tellurates with monolayered structures becomes weaker with increasing interslab distance between the magnetic (Te, M)–O layers [see ESI,† Fig. S1]. Although the ionic radius of Ag^+ is smaller than that of K^+,[38] the interslab distance between the (Te, M)–O honeycomb layers in $Ag_{2-x}M_2TeO_6$ is comparable to $K_2M_2TeO_6$ due to a straight dumbbell-like coordination between Ag^+ and O^{2-} ions,[27] confirming the suppression of the interslab magnetic exchange coupling by interslab distance rather than ionic radius. The formation of Ag-bilayers with the straight coordination in $Ag_6M_2TeO_6$ realizes even a longer interslab distance of approximately 9 Å – the longest amongst all the experimentally reported honeycomb layered tellurates. Thus, the large interslab distance screening the interslab magnetic exchange coupling is the most likely candidate responsible for the signatures of the 2D spin-frustrated state.

Conclusion

In conclusion, we have investigated magnetic properties of Ag-based honeycomb tellurates: $Ag_2M_2TeO_6$ (M = Co, $Co_{0.5}Ni_{0.5}$, and Ni), in which a large interslab distance due to Ag-bilayers with straight coordination suppresses the interslab magnetic exchange coupling of (Te, M)–O magnetic honeycomb layers. From temperature and field dependent magnetization measurements, antiferromagnetic ordering and a signature of spin-frustration have been observed for all the samples. Although studies on single-crystals are necessary to further clarify and optimize the magnetic properties, the results suggest that Ag-based honeycomb layered tellurates might be promising for the realization of strong spin-frustration and the Kitaev quantum spin liquid.[39] Synthesis of epitaxial heterostructures recently reported for honeycomb layered oxides[37] could be employed to obtain single-crystals, which could offer further insights and controllability of spin textures in Ag-based honeycomb layered tellurates.

Methods

Polycrystalline powders of $Ag_2M_2TeO_6$ (M = Co, $Co_{0.5}Ni_{0.5}$, and Ni) are prepared by a low temperature ion-exchange reaction: $Na_2M_2TeO_6 + 2AgNO_3 \rightarrow Ag_2M_2TeO_6 + 2NaNO_3$. The $Na_2M_2TeO_6$ precursors are reacted with a molten flux of a 4-fold molar excess amount of $AgNO_3$. The residual nitrates were dissolved in distilled water. Further details on the sample synthesis are described elsewhere.[28] Magnetic properties of the samples are characterized using a Quantum Design Magnetic Property Measurement System with a temperature-range of 2–300 K and a magnetic field-range of ± 70 kOe. The crystal structures in ESI† are visualized by the VESTA program.[40]

Author contributions

S. K., K. T., and T. M. conceived and designed the experiments. S. K. performed magnetization measurements on the samples prepared by T. M. K. T. performed model calculation. N. T. performed TEM characterization. S.K. performed the data analysis with inputs from K. T., N. T., T. T., and T. M. All authors discussed the results and commented on the manuscript, which was written by S. K.

Conflicts of interest

The authors declare no competing financial interest.

Acknowledgements

S. K. and T. T. acknowledge funding from the JST FOREST Grant (No. JPMJFR212V) and JSPS KAKENHI Grant (No. 20K23374 and 21H04614). T. M. acknowledges funding from Iketani Science and Technology and AIST-Ritsumeikan University University Fusion Seeds Sprout Program. K. T. acknowledges funding from the JSPS KAKENHI Grant (No. 20K15177).

References

1 L. Balents, *Nature*, 2010, **464**, 199–208.
2 L. Savary and L. Balents, *Rep. Prog. Phys.*, 2017, **80**, 016502.
3 A. Kitaev, *Ann. Phys.*, 2006, **321**, 2–111.
4 H. Takagi, T. Takayama, G. Jackeli, G. Khaliullin and S. E. Nagler, *Nat. Rev. Phys.*, 2019, **1**, 264–280.

5 G. M. Kanyolo, T. Masese, N. Matsubara, C.-Y. Chen, J. Rizell, Z.-D. Huang, Y. Sassa, M. Månsson, H. Senoh and H. Matsumoto, *Chem. Soc. Rev.*, 2021, **50**, 3990–4030.
6 Y. Motome and J. Nasu, *J. Phys. Soc. Jpn.*, 2020, **89**, 012002.
7 S. H. Do, S. Y. Park, J. Yoshitake, J. Nasu, Y. Motome, Y. S. Kwon, D. T. Adroja, D. J. Voneshen, K. Kim, T. H. Jang, J. H. Park, K. Y. Choi and S. Ji, *Nat. Phys.*, 2017, **13**, 1079–1084.
8 G. Khaliullin, *Prog. Theor. Phys. Suppl.*, 2005, **160**, 155–202.
9 G. Jackeli and G. Khaliullin, *Phys. Rev. Lett.*, 2009, **102**, 017205.
10 K. W. Plumb, J. P. Clancy, L. J. Sandilands, V. V. Shankar, Y. F. Hu, K. S. Burch, H. Kee and Y. Kim, *Phys. Rev. B*, 2014, **90**, 041112(R).
11 Y. Motome, R. Sano, S. Jang and Y. Sugita, *J. Phys.: Condens. Matter*, 2020, **32**, 404001.
12 H. Liu, J. Chaloupka and G. Khaliullin, *Phys. Rev. Lett.*, 2020, **125**, 047201.
13 A. L. Sanders, R. A. Mole, J. Liu, A. J. Brown, D. Yu, C. D. Ling and S. Rachel, *Phys. Rev. B*, 2022, **106**, 014413.
14 C. Kim, J. Jeong, G. Lin, P. Park, T. Masuda, S. Asai, S. Itoh, H. Kim, H. Zhou, J. Ma and J. Park, *J. Phys.: Condens. Matter*, 2022, **34**, 045802.
15 R. Berthelot, W. Schmidt, A. W. Sleight and M. A. Subramanian, *J. Solid State Chem.*, 2012, **196**, 225–231.
16 L. Viciu, Q. Huang, E. Morosan, H. W. Zandbergen, N. I. Greenbaum, T. McQueen and R. J. Cava, *J. Solid State Chem.*, 2007, **180**, 1060–1067.
17 E. Lefrançois, M. Songvilay, J. Robert, G. Nataf, E. Jordan, L. Chaix, C. V. Colin, P. Lejay, A. Hadj-Azzem, R. Ballou and V. Simonet, *Phys. Rev. B*, 2016, **94**, 214416.
18 A. K. Bera, S. M. Yusuf, A. Kumar and C. Ritter, *Phys. Rev. B*, 2017, **95**, 094424.
19 A. M. Samarakoon, Q. Chen, H. Zhou and V. O. Garlea, *Phys. Rev. B*, 2021, **104**, 184415.
20 T. Murtaza, R. Kalaivanan, G. Madeswaran, K. Bayikadi and R. Sankar, *J. Mater. Res. Technol.*, 2021, **14**, 1601–1608.
21 S. K. Karna, Y. Zhao, R. Sankar, M. Avdeev, P. C. Tseng, C. W. Wang, G. J. Shu, K. Matan, G. Y. Guo and F. C. Chou, *Phys. Rev. B*, 2017, **95**, 104408.
22 R. Sankar, I. Panneer Muthuselvam, G. J. Shu, W. T. Chen, S. K. Karna, R. Jayavel and F. C. Chou, *CrystEngComm*, 2014, **16**, 10791–10796.
23 A. I. Kurbakov, A. N. Korshunov, S. Y. Podchezertsev, M. I. Stratan, G. V. Raganyan and E. A. Zvereva, *J. Alloys Compd.*, 2020, **820**, 153354.
24 A. K. Bera, S. M. Yusuf, L. Keller, F. Yokaichiya and J. R. Stewart, *Phys. Rev. B*, 2022, **105**, 014410.
25 N. Matsubara, E. Nocerino, O. K. Forslund, A. Zubayer, K. Papadopoulos, D. Andreica, J. Sugiyama, R. Palm, Z. Guguchia, S. P. Cottrell, T. Kamiyama, T. Saito, A. Kalaboukhov, Y. Sassa, T. Masese and M. Månsson, *Sci. Rep.*, 2020, **10**, 18305.
26 T. Vasilchikova, A. Vasiliev, M. Evstigneeva, V. Nalbandyan, J. S. Lee, H. J. Koo and M. H. Whangbo, *Materials*, 2022, **15**, 2563.
27 K. Tada, T. Masese and G. Mbiti, *Comput. Mater. Sci.*, 2022, **207**, 111322.
28 T. Masese, G. M. Kanyolo, Y. Miyazaki, M. Ito, N. Taguchi, J. Rizell, S. Tachibana, K. Tada, Z.-D. Huang, A. Alshehabi, H. Ubukata, K. Kubota, K. Yoshii, H. Senoh, C. Tassel, Y. Orikasa, H. Kageyama and T. Saito, *Adv. Sci.*, 2022, 2204672.
29 M. Mecklenburg and B. C. Regan, *Phys. Rev. Lett.*, 2011, **106**, 116803.
30 N. Rogado, Q. Huang, J. W. Lynn, A. P. Ramirez, D. Huse and R. J. Cava, *Phys. Rev. B: Condens. Matter Mater. Phys.*, 2002, **65**, 144443.
31 W. Chen, X. Li, Z. Hu, Z. Hu, L. Yue, R. Sutarto, F. He, K. Iida, K. Kamazawa, W. Yu, X. Lin and Y. Li, *Phys. Rev. B*, 2021, **103**, L180404.
32 H. N. N. Teo, A. Korshunov, I. Sa and A. Kurbakov, *Phys. Status Solidi B*, 2020, **257**, 1900232.
33 I. Kimchi, J. P. Sheckelton, T. M. McQueen and P. A. Lee, *Nat. Commun.*, 2018, **9**, 4367.
34 I. Kimchi, A. Nahum and T. Senthil, *Phys. Rev. X*, 2018, **8**, 031028.
35 K. Kitagawa, T. Takayama, Y. Matsumoto, A. Kato, R. Takano, Y. Kishimoto, S. Bette, R. Dinnebier, G. Jackeli and H. Takagi, *Nature*, 2018, **554**, 341–345.
36 S. H. Do, C. H. Lee, T. Kihara, Y. S. Choi, S. Yoon, K. Kim, H. Cheong, W. T. Chen, F. Chou, H. Nojiri and K. Y. Choi, *Phys. Rev. Lett.*, 2020, **124**, 47204.
37 B. Kang, M. Park, S. Song, S. Noh, D. Choe, M. Kong, M. Kim, C. Seo, E. K. Ko, G. Yi, J. Yoo, S. Park, J. M. Ok and C. Sohn, *Phys. Rev. B*, 2023, **107**, 075103.
38 R. D. Shannon, *Acta Cryst.*, 1976, **A32**, 751–767.
39 C. Nayak, S. H. Simon, A. Stern and M. Freedman, *Rev. Mod. Phys.*, 2008, **80**, 1083–1159.
40 K. Momma and F. Izumi, *J. Appl. Cryst.*, 2011, **44**, 1272–1276.